# Analysis of Electrostatics and Correlated Motions for Hydride Transfer in Dihydrofolate Reductase

**Kim F. Wong, James B. Watney, and Sharon Hammes-Schiffer***

*Department of Chemistry, 152 Davey Laboratory, The Pennsylvania State University, University Park, Pennsylvania 16802*

The hydride transfer reaction catalyzed by the enzyme dihydrofolate reductase is simulated with a hybrid quantum/classical molecular dynamics method. Electronic and nuclear quantum effects, as well as the motion of the entire solvated enzyme, are included in these simulations. The free energy profile is generated as a function of a collective reaction coordinate. The structure, hydrogen bonding, electrostatic interactions, and correlated motions are analyzed along the collective reaction coordinate (i.e., at the reactant, transition state, and product). The analysis of hydrogen bonding and electrostatics provides insight into the impact of conformational changes on the energetics of the reaction. A charge deletion scheme is used to quantify the electrostatic contributions of each residue along the collective reaction coordinate and to identify the key residues that influence the changes in the electrostatic energy during the reaction. Analysis of the correlated motions in the enzyme, cofactor, and substrate reveals significant changes in the correlations during the reaction and identifies the correlated motions most relevant to hydride transfer. These analyses have important implications for protein engineering and drug design.

## I. Introduction

Dihydrofolate reductase (DHFR) is required for normal folate metabolism in prokaryotes and eukaryotes. This enzyme catalyzes the reduction of 7,8-dihydrofolate (DHF) to 5,6,7,8-tetrahydrofolate (THF) using nicotinamide adenine dinucleotide phosphate (NADPH) as a coenzyme.[1] In this reaction, the pro-*R* hydride of NADPH is transferred to the C6 of the pterin substrate with concurrent protonation at the N5 position. The product, THF, is essential for the biosynthesis of purines, pyrimidines, and amino acids. As a result, DHFR has been fostered as a pharmacological target and has been studied extensively with a wide range of experimental and theoretical approaches.

Kinetic studies of *Escherichia coli* DHFR have been used to determine the entire kinetic mechanism for DHFR.[1,2] These kinetic studies have been applied to single and multiple mutants,[3-7] as well as to the wild-type enzyme. The mechanism of the proton and hydride transfer reactions catalyzed by DHFR has been the subject of several theoretical investigations. Combined quantum mechanical/molecular mechanical (QM/MM) calculations suggest that the protonation of DHF facilitates the hydride transfer reaction.[8] Analysis of the hydrogen bonding distances between water molecules and the N5 position in classical molecular dynamics simulations has been used to postulate a mechanism in which the hydride transfer occurs prior to the proton transfer.[9,10] Recent calculations[11] provide more direct evidence that the reaction proceeds through an initial proton transfer followed by a hydride transfer. The calculations in the present paper focus on the hydride transfer reaction from NADPH to the protonated substrate, as depicted in Figure 1.

The minima and transition states for the hydride transfer reaction catalyzed by DHFR have been studied with semiem-pirical, ab initio, and QM/MM methods.[12-15] Early semiempirical and ab initio calculations were performed for small model systems in the gas phase,[12-14] and semiempirical QM/MM geometry optimizations were performed to identify the transition state for hydride transfer in the presence of the enzyme.[15] More recently, a QM/MM method was combined with molecular dynamics to estimate the activation free energy for the hydride transfer reaction.[16] Classical molecular dynamics with a QM/MM potential were also used to study the effects of the enzyme electric field on the electronic polarization of the substrate during hydride transfer.[17]

Both experimental and theoretical studies have provided insight into the structure and conformational motions of DHFR. X-ray crystallographic structures illustrate that the *E. coli* DHFR enzyme assumes different conformations along the reaction pathway.[18] NMR relaxation experiments indicate that the binding of the substrate and coenzyme alters the motion of the enzyme in regions far from the binding sites, as well as in the active site.[19-21] Classical molecular dynamics simulations have been used to investigate the domain motions and conformational changes relevant to hydride transfer in DHFR.[9,22-24] Classical molecular dynamics simulations identified strong correlated and anticorrelated motions involving spatially distinct regions for the reactant ternary complex with DHF but not for the product complexes with THF, implying that these motions might be tied to catalysis.[23] These correlated and anticorrelated motions involve many of the same regions of the protein implicated by dynamic NMR measurements.[19,20] Recent simulations indicate that these correlated motions are reduced in mutant DHFR enzymes with significantly slower hydride transfer rates,[24] suggesting the importance of long-range structural perturbations created by the mutations.

Previously, we studied hydride transfer in *E. coli* DHFR with a hybrid quantum/classical molecular dynamics approach.[25-27] The potential energy surface was described with a two-state

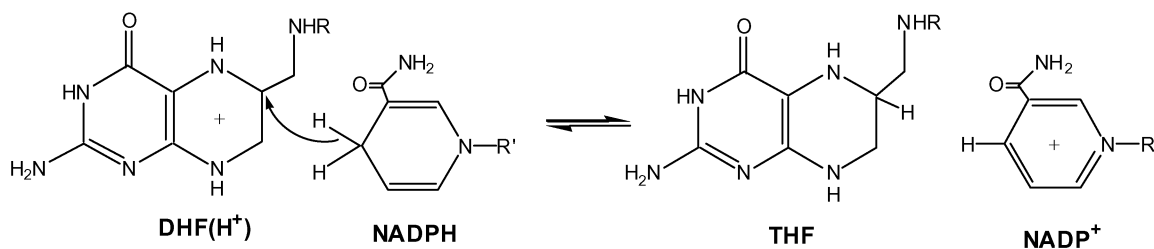* Author to whom corresspondence should be addressed. E-mail: shs@chem.psu.edu.

**Figure 1.** The hydride transfer reaction from the NADPH cofactor to the protonated DHF substrate.

empirical valence bond (EVB) model[28] parametrized to reproduce the experimental free energies of activation and reaction.[2] The hydride transfer rate was expressed as the product of a transition state theory rate constant that depends on the activation free energy barrier and a transmission coefficient that accounts for barrier recrossings. The free energy profile was generated as a function of a collective reaction coordinate with umbrella sampling techniques, and the transmission coefficient was calculated with a reactive flux scheme. The nuclear quantum effects, such as zero point energy and hydrogen tunneling, as well as the motion of the entire solvated enzyme, were included during the calculation of the free energy profile and the transmission coefficient.[29,30] The nuclear quantum effects were found to lower the free energy barrier by 2−3 kcal/mol.[25] The calculated deuterium kinetic isotope effect was consistent with the experimental value of 3, and hydrogen tunneling in the direction along the donor−acceptor axis was found to be significant.[25] The transmission coefficient was calculated to be ∼0.88.[25]

Analysis of these quantum/classical molecular dynamics simulations provided evidence for a network of coupled promoting motions extending throughout the protein and ligands, where promoting motions refer to equilibrium, thermally averaged conformational changes along the collective reaction coordinate, leading to configurations conducive to the reaction.[25−27,31] The equilibrium molecular motions in this network are not dynamically coupled in real time to the chemical transformation of the substrate and cofactor. These equilibrium motions are averaged over the fast vibrational modes and reflect conformational changes occurring on the much slower millisecond time scale of the overall hydride transfer reaction. The motions in this network give rise to conformations of the ternary complex in which the hydride transfer reaction is facilitated because of short transfer distances, suitable orientation of substrate and cofactor, and a favorable electrostatic environment for charge transfer. The results of the application of this approach to a mutant DHFR enzyme are consistent with the experimental rate measurements and suggest that the mutation may modify the network of coupled motions through structural perturbations, thereby increasing the free energy barrier and decreasing the reaction rate.[27] These results imply that long-range structural perturbations caused by a distal mutation can influence the conformational motions of the enzyme along the reaction coordinate in a manner that significantly alters the free energy barrier.

Recently Garcia-Viloca and co-workers used a QM/MM approach with semiclassical tunneling contributions to study hydride transfer in DHFR.[11] The potential energy surface was modeled with a semiempirical QM/MM method that was augmented with a simple valence-bond term parametrized to reproduce the experimental free energies of reaction and activation. The free energy profile was generated with umbrella sampling techniques on the basis of 40 ps of molecular dynamics for 18 windows along the reaction coordinate, leading to a total

of 0.72 ns of sampling after equilibration. The nuclear quantum effects were included with the ensemble-averaged variational transition state theory with semiclassical multidimensional tunneling contributions. The decrease in the free energy barrier resulting from nuclear quantum effects and the transmission coefficient corresponding to barrier recrossings were similar to the values calculated in ref 25. The calculated primary deuterium kinetic isotope effect was consistent with the experimental value, as well as the value calculated previously.[25] The variations of key distances along the reaction path were found to be similar to those obtained in ref 25.

In another recent study, Thorpe and Brooks used an alternative approach to study hydride transfer in DHFR.[32] In this approach, the potential energy surface was modeled with a semiempirical QM/MM method without the addition of the correction terms implemented by Garcia-Viloca and co-workers.[11] The structures used in this study were obtained from a 10 ns classical molecular dynamics simulation of the reactant state. A subset containing 284 of the configurations in which the hydrogen−acceptor distance was less than or equal to 2.5 Å was chosen for the QM/MM calculations. (Note that the typical hydrogen−acceptor distances of ∼1.5 Å in the transition state for hydride transfer were not attainable because only the reactant state was sampled.) For each reactant configuration in this subset, a reaction path for hydride transfer was obtained by performing a QM/MM optimization for a series of fixed hydrogen−acceptor distances as the transferring hydrogen was moved from the donor to the acceptor. Only the two ligands and solvent atoms within 10 Å of the transferring hydrogen were allowed to move during these optimizations (i.e., the entire protein was fixed). The nuclear quantum effects, such as zero point motion and hydrogen tunneling, as well as the dynamical barrier recrossing effects, were neglected in this study. The resulting set of energy barriers was used to estimate the hydride transfer free energy barrier, which is in agreement with the experimentally determined value. The authors observed similar variations along the reaction path for the distances comprising the network of coupled motions identified previously[25,26] and also concluded that equilibrium enzyme motions are important with respect to conformational changes that facilitate hydride transfer.

In the present paper, we extend the length of our hybrid quantum/classical molecular dynamics simulations and analyze the changes in hydrogen bonding, electrostatic interactions, and correlated motions during the hydride transfer reaction. In our initial calculations of DHFR,[25,26] the free energy profile was generated with umbrella sampling techniques based on 140 ps of molecular dynamics for 11 windows along the collective reaction coordinate, leading to a total of 1.54 ns of sampling after equilibration. In the present paper, the free energy profile is generated with 4.5 ns of molecular dynamics for 20 windows along the collective reaction coordinate, leading to a total of 90 ns of sampling. Previously,[23,24] the correlation matrix was studied for the reactant and product but not for the transition

Hydride Transfer in Dihydrofolate Reductase

*J. Phys. Chem. B, Vol. 108, No. 32, 2004* **12233**

state. Here, we analyze the correlation matrix for the transition state, as well as the reactant and product, to identify the changes in correlated motions most relevant to hydride transfer. The accompanying analysis of hydrogen bonding and electrostatics along the collective reaction coordinate provides insight into the impact of conformational changes on the energetics of the reaction.

## II. Methodology

The hybrid quantum/classical molecular dynamics method for simulating proton- and hydride transfer reactions in enzymes has been presented in full detail elsewhere.[29] The present study focuses on only equilibrium thermally averaged properties of the hydride transfer reaction and does not include calculations of the transmission coefficient, which accounts for dynamical barrier recrossings. Since the transmission coefficient has been found to be near unity for DHFR,[25] dynamical effects should not significantly influence the results presented here. Central to our analysis is the generation of an adiabatic quantum free energy profile from molecular dynamics trajectories governed by a series of mapping potentials. In this section, we briefly summarize the hybrid quantum/classical molecular dynamics approach for computing the adiabatic free energy profile for hydride transfer and describe the analyses of the electrostatics and the correlated fluctuations.

**A. Hybrid Quantum/Classical Molecular Dynamics.** A two-state EVB potential is used to describe the breaking and forming of chemical bonds on the electronic ground state potential energy surface. In VB state 1, the hydride is bonded to the donor, whereas in VB state 2, the hydride is bonded to the acceptor. The diagonal elements of the $2 \times 2$ EVB Hamiltonian are described by the GROMOS force field 43A1[33] with a few modifications. One of these changes is the explicit treatment of the hydrogen atoms that are bound to the donor and acceptor, in contrast to the united-atom GROMOS force field.[33] Furthermore, a Morse potential is included to describe the bonding of the transferring hydride with the donor or acceptor carbon. The coupling, $V_{12}$, between the two VB states and the constant energy adjustment, $\Delta_{12}$, to the second VB state are chosen to ensure that the adiabatic quantum free energy profile for the hydride transfer reaction reproduces the experimentally determined free energy barriers for the forward and reverse rates of hydride transfer in wild-type DHFR.[2] The values determined for these parameters are $V_{12} = 34.66$ kcal/mol and $\Delta_{12} = 65.25$ kcal/mol. (Note that these parameters have been refined slightly since the previous simulations.)

In this hybrid quantum/classical molecular dynamics approach, the transferring hydrogen nucleus is treated quantum-mechanically, while the other nuclei are treated classically. The classical subsystem is propagated according to classical molecular dynamics. The nuclear quantum effects of the transferring hydrogen are included in the molecular dynamics simulations[34,35] by calculating the adiabatic vibrational nuclear wave functions for each sampled classical configuration:

$$[T_H + V_{el0}(\mathbf{r},\mathbf{R})]\Phi_j(\mathbf{r};\mathbf{R}) = \epsilon_j(\mathbf{R})\Phi_j(\mathbf{r};\mathbf{R}) \qquad (1)$$

where $\mathbf{r}$ denotes the hydrogen nuclear coordinate, $\mathbf{R}$ denotes the classical nuclear coordinates, $T_H$ is the kinetic energy of the hydrogen nucleus, and $V_{el0}$ is the EVB potential energy of the electronic ground state.

The free energy profile is evaluated as a function of a collective reaction coordinate that is analogous to the solvent coordinate used in standard Marcus theory for electron transfer

reactions.[36-39] This collective reaction coordinate is defined as

$$\Lambda(\mathbf{R}) = \langle\Phi_0(\mathbf{r};\mathbf{R})|V_{11}(\mathbf{r},\mathbf{R}) - V_{22}(\mathbf{r},\mathbf{R})|\Phi_0(\mathbf{r};\mathbf{R})\rangle_{\mathbf{r}} \quad (2)$$

where $V_{11}(\mathbf{r},\mathbf{R})$ and $V_{22}(\mathbf{r},\mathbf{R})$ represent the energies of VB states 1 and 2 (i.e., the diagonal elements of the EVB Hamiltonian) and $\Phi_0(\mathbf{r};\mathbf{R})$ is the wave function corresponding to the hydrogen vibrational ground state. This choice of reaction coordinate has been shown to be physically meaningful for two-state charge-transfer reactions.[40,41] Moreover, previous simulations of enzymatic reactions[25,29] indicate that this reaction coordinate is justified from a transition state theory perspective because the estimates of the recrossing transmission coefficient are close to unity.

A series of mapping potentials is used to bias the molecular dynamics for efficient sampling of the relevant range of the collective reaction coordinate. These mapping potentials are defined to be linear combinations of the two VB states:

$$V_{map}(\mathbf{r},\mathbf{R};\lambda) = (1 - \lambda)V_{11}(\mathbf{r},\mathbf{R}) + \lambda V_{22}(\mathbf{r},\mathbf{R}) \qquad (3)$$

The reaction progresses from the reactant VB state 1 to the product VB state 2 as the mapping parameter, $\lambda$, is varied from zero to unity. Molecular dynamics simulations governed by these mapping potentials are used in conjunction with a standard binning procedure to determine segments of the free energy profile. The individual pieces of the free energy profile are connected by thermodynamic integration, thus enabling the generation of the entire adiabatic quantum free energy profile along the reaction coordinate. The nuclear quantum effects of the transferring hydrogen are included with the perturbation formula derived in ref 29.

The system employed in our DHFR calculations contains the protein, an NADPH cofactor, a protonated DHFR substrate, and 4122 water molecules in a truncated octahedral periodic box with a distance of 66.61 Å between opposing square faces. The initial coordinates were obtained from a crystal structure of *E. coli* DHFR complexed with NADPH$^+$ and folate (PDB code 1rx2).[18] In this crystal structure, the Met20 loop is in the closed configuration, which is thought to be the active form for the hydride transfer reaction. The reaction studied is the transfer of the pro-*R* hydrogen on the donor carbon of NADPH to the acceptor carbon of the protonated DHF. We used a set of 20 mapping parameters, ($\lambda = 0.000, 0.025, 0.050, 0.088, 0.125, 0.188, 0.250, 0.313, 0.375, 0.438, 0.500, 0.563, 0.625, 0.688, 0.750, 0.813, 0.875, 0.913, 0.950, 0.975$) and performed 4.5 ns of molecular dynamics for each window. As discussed below, 2 ns of additional sampling (for $\lambda = 0.375, 0.438, 0.500, 0.563$) were performed near the transition state region to obtain 98 ns of total sampling.

In this paper, we analyze properties of the reactant state (RS), the product state (PS), and the transition state (TS). The RS and PS ensembles are comprised of the configurations within ±2.5 kcal/mol of the free energy minimum for the reactant and product, respectively. Similarly, the transition state (TS) ensemble is comprised of the configurations within ±2.5 kcal/mol of the free energy maximum. We used an iterative scheme to determine the average structures for the RS, TS, and PS ensembles. First, all configurations of an ensemble were translated and rotated to minimize the root-mean-square deviation of the $C_\alpha$ atoms with respect to an arbitrary configuration in the ensemble. Then, this procedure was repeated with respect to the average configuration from the previous iteration. This procedure was iterated until convergence of the average structure within a specified tolerance.

**12234** *J. Phys. Chem. B, Vol. 108, No. 32, 2004*

Wong et al.

**B. Electrostatic Analysis.** The electrostatic potential was calculated by solving the linearized Poisson−Boltzmann equation using the DelPhi program.[42,43] To be consistent with the molecular dynamics simulations, atomic charges and atomic radii were taken from the GROMOS 43A1 force field.[33] The atomic charge, $q$, for a given atom is taken as a linear combination of that atom's charge in VB state 1 and VB state 2:

$$q = (c_{11})^2 q_1 + (c_{21})^2 q_2 \qquad (4)$$

where $q_1$ is the atomic charge for the atom in VB state 1, $q_2$ is the atomic charge for the atom in VB state 2, and $c_{11}$ and $c_{21}$ are the coefficents of the normalized ground state EVB wave function. The atomic radius $r_{at}$ for each atom was calculated from the Lennard−Jones parameters $C_{12}$ and $C_6$ using the following relation:

$$2r_{at} = (2C_{12}/C_6)^{1/6} \qquad (5)$$

Dielectric constants of $\epsilon = 80$ and $\epsilon = 4$ were used for solvent and solute, respectively.

**C. Covariance Analysis.** The statistical correlation between the fluctuation of residue $j$ with the fluctuation of residue $k$ is given by the cross-correlation matrix[44,45]

$$S_{jk} = \frac{C_{jk}}{(C_{jj}C_{kk})^{1/2}} \qquad (6)$$

where

$$C_{jk} = \langle (\mathbf{r}_j - \langle \mathbf{r}_j \rangle) \cdot (\mathbf{r}_k - \langle \mathbf{r}_k \rangle) \rangle \qquad (7)$$

defines the covariance of the two fluctuations, and the brackets denote an ensemble average over configurations. Since this covariance matrix is constructed as the dot product of fluctuation vectors rather than the scalar product of the components, $C$ is an $N \times N$ matrix representing the correlation between the fluctuations of the N atoms. This matrix describes pairwise atomic motions that are either in phase (i.e., moving in the same direction) or out of phase (i.e., moving in opposite directions). Note that this matrix does not characterize correlated fluctuations that are orthogonal to each other because the dot product of these fluctuations is zero.

We verified that the covariance matrix elements are converged within the time scale of the simulations. For the reactant and product ensembles, the cross-correlation matrix is similar for the first and second halves of the 4.5 ns of sampling, indicating that the corresponding coupled motions are valid equilibrium properties occurring on the nanosecond time scale. For the transition state ensemble, however, we observed more significant differences between the first and second halves of the 4.5 ns of sampling, although the middle portion of the 4.5 ns agrees with the matrix from the full 4.5 ns of sampling. Therefore, we performed an additional 2 ns of sampling in the TS region for each of the relevant four mapping potentials ($\lambda = 0.375$, 0.438, 0.500, 0.563). The cross-correlation matrix for this ensemble comprised of sets of 6.5 ns of MD is identical to that from the initial 4.5 ns sampling, indicating convergence of the 4.5 ns ensemble.

**III. Results and Discussion**

**A. Structural and Hydrogen Bonding Analysis.** Conformational changes along the reaction coordinate have been shown to facilitate the hydride transfer reaction catalyzed by
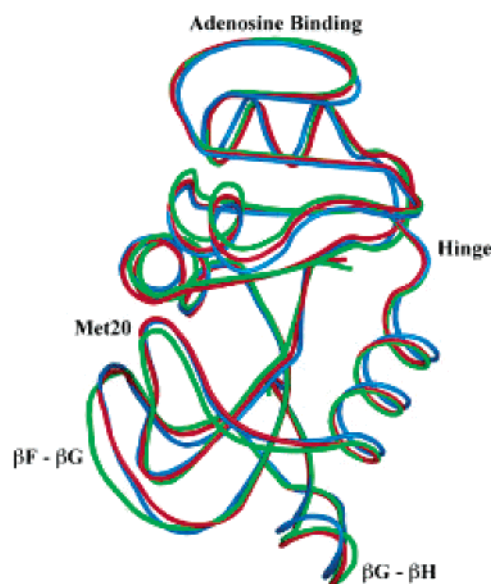


**Figure 2.** Thermally averaged structures of DHFR for the RS (green), TS (red), and PS (blue). The relevant loop regions are labeled. This figure was created using PyMol.[49]
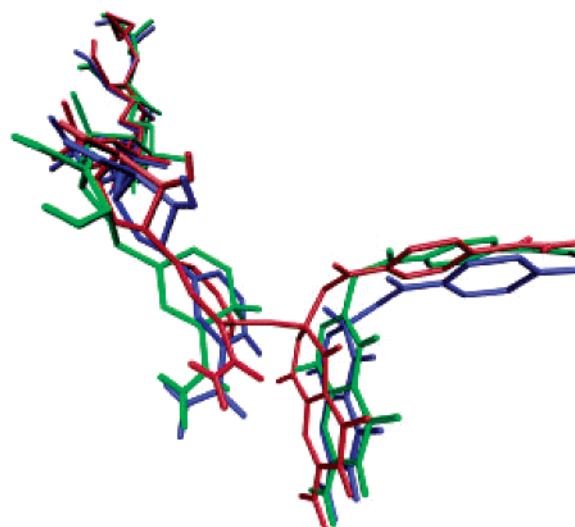


**Figure 3.** Thermally averaged structures of the cofactor (left) and the substrate (right) for the RS (green), TS (red), and PS (blue). This figure was created using VMD.[50]

DHFR.[11,24−26] Figure 2 depicts the thermally averaged structures of DHFR for the RS, TS, and PS ensembles. The three structures are qualitatively similar in that the key elements of the $\alpha$ helices and the $\beta$ sheets are intact. Significant differences are evident, however, in the loop regions, particularly in the $\beta$F−$\beta$G and Met20 loops. Figure 3 depicts the average structures of the cofactor and substrate for the RS, TS, and PS ensembles. The primary conformational change along the reaction coordinate is the rotation of the nicotinamide ring relative to the substrate. The tail ring of DHF is also oriented differently in the three structures. The latter observation is consistent with the previous analysis of the thermally averaged changes along the collective reaction coordinate for the angle between the acceptor carbon and the methylene amino linkage in the substrate.[26] The TS and PS average structures for the cofactor are more similar to each other than either one is to the RS average structure for the cofactor.

These conformational changes are also reflected in the hydrogen bond populations for each ensemble. The hydrogen
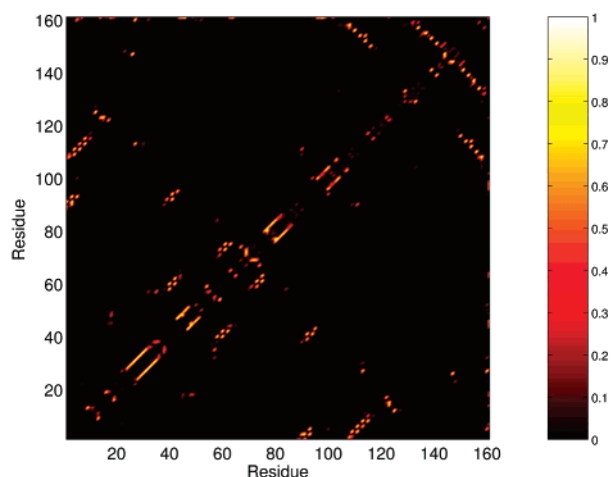
**Figure 4.** Hydrogen bond population for the TS ensemble of configurations. The hydrogen bond population between two residues is the fraction of configurations in the ensemble with hydrogen bonds between these two residues.

bond population between two residues in a given ensemble is the fraction of configurations with hydrogen bonds between these two residues, where a hydrogen bond is defined to have a maximum hydrogen−acceptor distance of 2.5 Å and a minimum donor−hydrogen−acceptor angle of 135°. Figure 4 depicts the hydrogen bond population for the TS ensemble. The majority of hydrogen bonds are preserved from RS to TS to PS, so we discuss only the differences among these ensembles. As the hydride transfer reaction progresses, the hydrogen bonds between the cofactor and Ser-63 and between the cofactor and Ala-7 break in the TS and form again in the PS. The hydrogen bond between the cofactor and Asn-18 breaks completely as the reaction evolves from RS to TS to PS. Other cases for which the hydrogen bond is present in the RS but absent in the PS include the interactions of Ser-3 with Glu-90, Glu-90 with Tyr-111, Gly-97 with Glu-101, Asp-132 with Arg-159, and

Asp-144 with Tyr-151. In addition, a number of hydrogen bonds are formed during the reaction. Hydrogen bonds that are absent in the RS but formed in the TS and PS include the interactions of Ile-14 with Thr-123, Gly-67 with Trp-74, and Asp-69 with Thr-73. These changes in the hydrogen bonding network influence the stability of the enzyme and thereby impact the energetics of the hydride transfer reaction.

**B. Electrostatic Analysis.** The conformational changes discussed in the previous subsection imply a reorganization of charge distribution during the reaction. In this subsection, we investigate the change in the electrostatic environment with two different types of electrostatic analyses. The first approach involves the calculation of the electrostatic potential by the solution of the linearized Poisson−Boltzmann equation for the RS, TS, and PS. The thermally averaged structures for these states were constructed as described above and are depicted in Figure 2. The second approach is a charge deletion scheme that provides the relative electrostatic interaction energy of each residue. The combination of these two types of analyses elucidates the changes in the charge distribution during hydride transfer.

Figure 5 depicts the electrostatic potential of the substrate and cofactor for the RS, TS, and PS. Of particular interest is the partial neutralization of charge on the N5 and C7 of the substrate as the reaction progresses from RS to TS to PS. As shown in Figure 5a, the positive charge on the pterin ring is completely gone in the PS. As shown in Figure 5b, the nicotinamide ring of the cofactor gradually gains a positive charge as the reaction evolves from RS to TS to PS. These observations are consistent with the charges assigned to the two VB states in the EVB potential.

Previous studies have shown the motion of the Met20 loop in DHFR to be involved in the catalytic cycle.[18,23] Our calculations reveal significant differences in the electrostatic potential at the molecular surface of the Met20 loop as the reaction progresses. Figure 6 depicts the electrostatic potential of the Met20 loop for the RS, TS, and PS. As shown in Figure
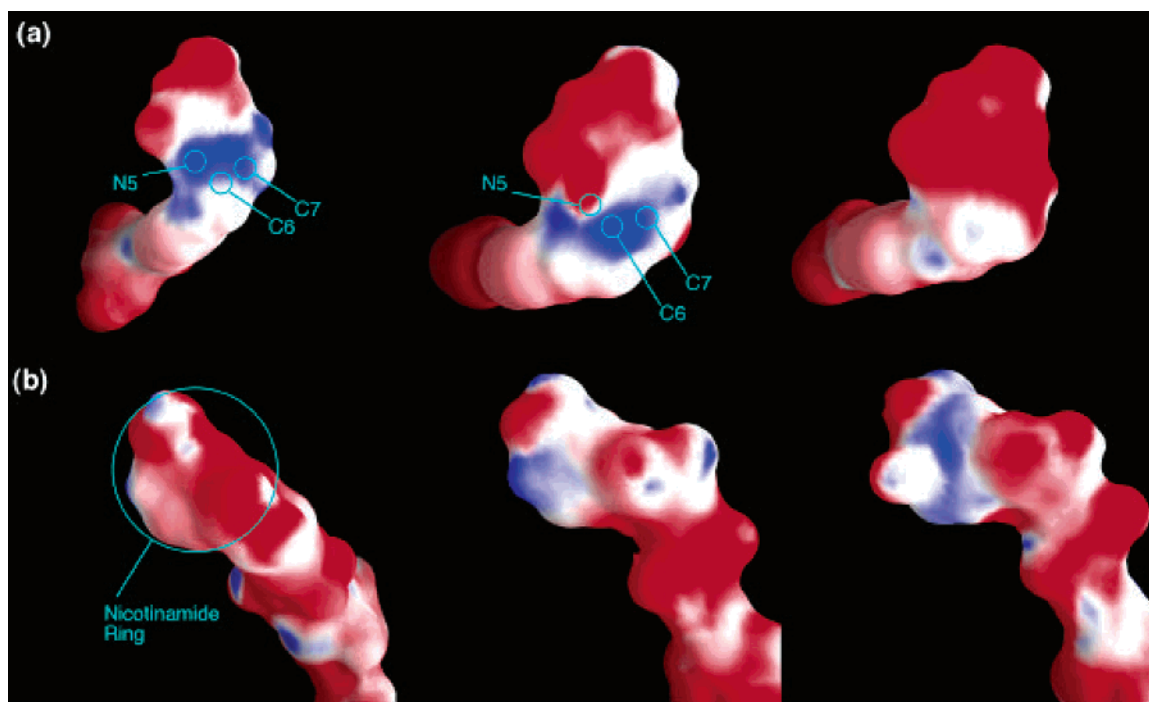


**Figure 5.** Electrostatic potential mapped to the molecular surface of the (a) substrate and (b) cofactor in the DHFR enzyme. The potentials are given for the RS (left), TS (middle), and PS (right). Blue indicates positive potential and red indicates negative potential. This figure was created using GRASP.[51,52]
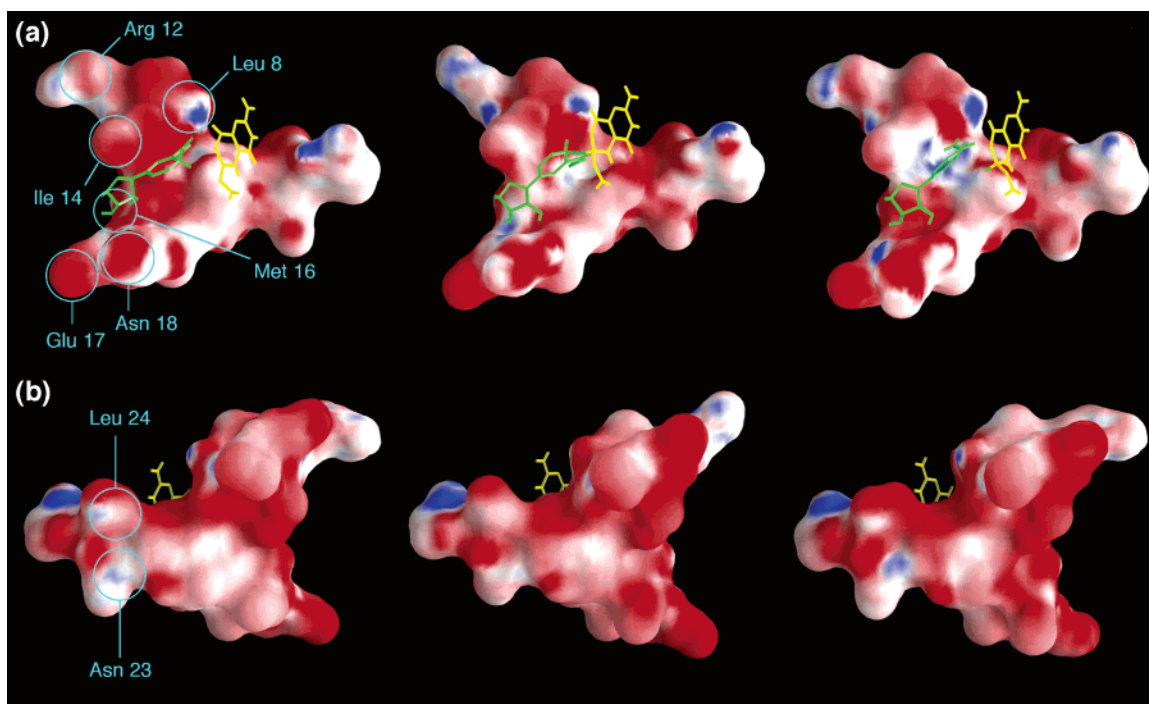
**Figure 6.** Electrostatic potential mapped to the molecular surface of the Met20 loop in DHFR for the RS (left), TS (middle), and PS (right). Blue indicates positive potential and red indicates negative potential. The substrate and cofactor are yellow and green, respectively. This figure was created using GRASP.[51,52]

6a, the side chain of Arg-12 moves as the reaction evolves from the RS to the TS and reverts to the original conformation in the PS. These conformational changes are accompanied by minor changes in the electrostatic potential. Other residues of the Met20 loop that exhibit a noticeable change in surface electrostatic potential include Ile-14, Met-16 and Asn-18. Ile-14 becomes more neutral progressing from RS to PS, Met-16 develops a positive charge only at the TS, and Asn-18 gradually develops a positive region as the reaction progresses from RS to PS. The most striking change in the Met20 loop is the change in electrostatic potential occurring in the pocket between Leu-8 and Ile-14: the potential in this pocket evolves from negative to positive as the reaction progresses from RS to PS. As shown in Figure 6b, two residues on the exterior of the loop also exhibit significant changes. The potential around Leu-24 changes from being partly positive in the RS to mostly negative in the TS and PS, and a region near Asn-23 is neutral at the TS but is positive in the RS and PS.

The $\beta$F$-\beta$G and $\beta$G$-\beta$H loop regions also exhibit significant changes in the electrostatic potential along the collective reaction coordinate. Figure 7 depicts the electrostatic potential for these loops for the RS, TS, and PS. For the $\beta$F$-\beta$G loop, the side chain of His-114 rotates as the reaction evolves from the RS to the TS and reverts to its orignal position in the PS. As shown in Figure 7a, a distinct region of positive surface electrostatic potential is observed near Phe-125 at the TS but is not observed in either the RS or the PS. Moreover, Thr-123 develops a region of positive potential that is present only in the PS. On the other side of the $\beta$F$-\beta$G loop, the side chain of Tyr-111 undergoes a modest conformational change as the reaction progresses from RS to TS and reverts to its original position in the PS. As shown in Figure 7b, the surface potential of Tyr-111 is much more neutral in the TS than in either the RS or the PS. The $\beta$G$-\beta$H loop shows significant changes in the electrostatic potential near residues 147−149. Four regions of positive surface potential near His-149, Ser-148, Ala-117, and Asn-147 are gradually neutralized as the reaction progresses from RS to PS.

To investigate the quantitative electrostatic contribution of each residue at the RS, TS, and PS, a charge deletion scheme is employed.[11,44] The electrostatic interaction energy of a given residue, $i$, is defined by subtracting the energy of the system when the atomic charges of residue $i$ are neutralized from the total energy of the system. Statistically meaningful interaction energies for the RS, TS, and PS are calculated by averaging the individual residue interaction energies over more than 2000 configurations for each ensemble. This definition of the interaction energy of a given residue differs from that of Garcia-Viloca and co-workers[11] in that Garcia-Viloca and co-workers include the interaction of residue $i$ with only the QM subsystem of their QM/MM simulation, whereas we include the interaction of residue $i$ with the entire system (i.e., protein, cofactor, substrate, and solvent). The charge deletion calculations were performed with two different cutoff distances (14 and 25 Å) in conjunction with the same reaction field. The results were found to be qualitatively similar for the two different cutoff distances. For consistency with the simulations that generated the equilibrium ensembles, the results are given for a cutoff distance of 14 Å with a reaction field.[25]

Table 1 presents the electrostatic contributions of each residue, $i$, at the TS and the PS relative to the RS, as well as the average distance between the C$_\alpha$ of residue $i$ and C6 of the substrate. For clarity, only residues with a change in electrostatic interaction energy greater than 2.0 kcal/mol in magnitude are given. These results indicate that nearly the same number of residues stabilize the TS (i.e., exhibit a negative change in electrostatic interaction energy) as destabilize the TS (i.e., exhibit a positive change in electrostatic interaction energy). The residues that exhibit a significant change in electrostatic interaction energies are distributed throughout the protein. The vast majority of the residues in Table 1 are located more than 10 Å from the C6 carbon of the substrate.

The analysis of the electrostatic contributions of residues in the loop regions is particularly relevant due to their perceived importance in catalysis. Only two residues from the Met20 loop,
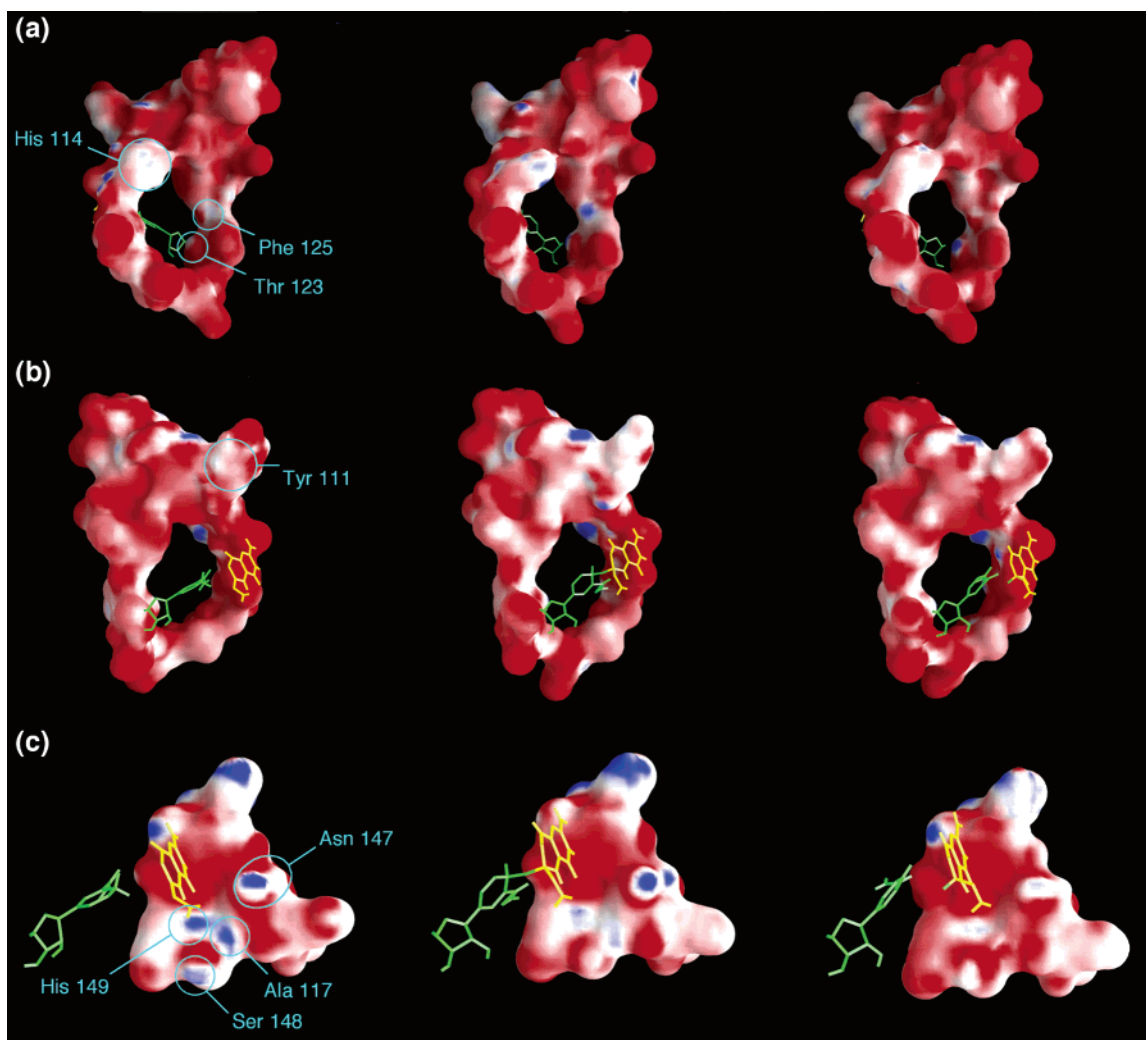
Hydride Transfer in Dihydrofolate Reductase

*J. Phys. Chem. B, Vol. 108, No. 32, 2004* **12237**



**Figure 7.** Electrostatic potential mapped to the molecular surface of the (a), (b) $\beta F-\beta G$ loop and (c) $\beta G-\beta H$ loop. The potentials are given for the RS (left), TS (middle), and PS (right). Blue indicates positive potential and red indicates negative potential. The substrate and cofactor are yellow and green, respectively. This figure was created using GRASP.[51,52]

Arg-12 and Glu-17, exhibit significant changes in their electrostatic interaction energies. These two residues have opposite effects at the TS: Arg-12 has a destabilizing effect, while Glu-17 has a stabilizing effect. The combined impact of these two residues is stabilizing at the TS and PS relative to the RS. Several residues associated with the $\beta F-\beta G$ loop region exhibit a significant effect: His-114, Asp-116, Gly-121, and Asp-122. His-114 has a stabilizing effect at the TS and a less pronounced stabilizing effect at the PS. Asp-116, Gly-121 and Asp-122 all have destabilizing effects at the TS that are amplified at the PS. The combined impact of these residues is destabilizing at the TS and at the PS relative to the RS. Finally, residues Asp-144, Gln-146, His-149, and Ser-150, which are all near the $\beta G-\beta H$ loop region, exhibit noticeable changes in their interaction energies. Asp-144 stabilizes both the TS and the PS. Gln-146 and Ser-150 both have destabilizing effects at the PS that are less pronounced at the TS. His-149 has a stabilizing effect at the TS that is less pronounced at the PS. Similar to the Met20 loop, these residues have a combined stabilizing effect at both the TS and the PS.

Recently, Garcia-Viloca and co-workers[11] also investigated DHFR using a charge deletion scheme. According to this previous study, those residues exhibiting a marked change in interaction energy upon going from RS to TS provide a stabilizing effect at the TS that is amplified at the PS. In contrast, our results indicate that only 12 of the 37 residues in Table 1

stabilize both the TS and the PS, with 9 of those 12 residues exhibiting an increased stabilization effect in the PS compared to the TS. Although Garcia-Viloca and co-workers did not identify many residues that destabilize the TS, we observe that 22 of 37 residues in Table 1 destabilize the TS, with 17 of those 22 exhibiting an increased destabilization effect in the PS. Therefore, the majority of residues that have the same effect in the TS as in the PS exhibit an increased effect in the PS.

Several of the residues identified in the charge deletion analysis were also identified in the linearized Poisson–Boltzmann analysis of the electrostatic potential. For example, residues Arg-12 and His-114 were associated with significant electrostatic changes in both analyses. The side chains of these residues were found to exhibit significant conformational changes along the collective reaction coordinate as well. Furthermore, residues His-149 and Glu-17 were identified by both types of analyses as exhibiting substantial electrostatic changes during the hydride transfer reaction. These analyses indicate that changes in the electrostatic charge distribution significantly impact the energetics of the hydride transfer reaction.

Recent experiments have demonstrated the effects of mutation on the rate of hydride transfer in DHFR. Although residues 121 and 122 are ~15 Å from the acceptor carbon atom, mutation of these residues was found to significantly decrease the rate of hydride transfer.[5-7] For example, mutation of Gly121 to Val

**12238** *J. Phys. Chem. B, Vol. 108, No. 32, 2004*

Wong et al.

**TABLE 1: Electrostatic Contribution of Specified Residues to the Stabilization (Negative Value) or Destabilization (Positive Value) of the TS and PS$^a$**

| residue no. | $R_{C_6, C_\alpha}$ [Å] | $\Delta\Delta E_{TS}$ [kcal/mol] | $\Delta\Delta E_{PS}$ [kcal/mol] |
|---|---|---|---|
| 3 | 13.3 | −1.6 | −2.2 |
| 12 | 13.9 | 1.8 | 2.8 |
| 17 | 14.0 | −3.4 | −5.3 |
| 27 | 9.8 | 7.9 | 3.2 |
| 31 | 7.6 | −0.3 | −2.9 |
| 35 | 10.5 | 0.9 | 5.7 |
| 38 | 14.5 | −2.0 | 0.6 |
| 45 | 11.1 | 0.7 | 3.3 |
| 46 | 7.5 | 0.4 | 2.2 |
| 57 | 13.6 | −1.1 | −2.0 |
| 59 | 12.5 | 2.8 | 2.9 |
| 70 | 20.9 | 3.7 | 3.9 |
| 71 | 18.6 | 2.5 | 1.7 |
| 76 | 20.4 | −2.2 | −5.0 |
| 80 | 21.3 | −1.2 | −2.2 |
| 87 | 23.4 | −3.7 | −3.7 |
| 90 | 16.9 | 3.0 | 1.5 |
| 92 | 10.8 | 1.2 | 2.1 |
| 94 | 5.6 | 1.0 | 3.0 |
| 95 | 6.7 | −3.6 | 0.5 |
| 96 | 7.7 | 1.0 | 2.4 |
| 100 | 11.2 | −6.0 | −12.1 |
| 102 | 16.3 | 1.9 | 3.4 |
| 103 | 15.1 | 0.9 | 3.2 |
| 114 | 13.3 | −2.9 | −0.9 |
| 116 | 17.0 | 0.6 | 5.7 |
| 121 | 14.9 | 1.6 | 2.1 |
| 122 | 15.2 | 6.0 | 10.1 |
| 129 | 22.0 | 2.0 | −0.7 |
| 141 | 19.5 | 3.1 | 2.9 |
| 144 | 21.5 | −3.7 | −5.8 |
| 146 | 18.8 | 1.4 | 2.1 |
| 149 | 17.6 | −3.0 | −1.5 |
| 150 | 18.1 | 0.3 | 2.3 |
| 154 | 15.4 | −2.3 | −6.0 |
| 157 | 19.8 | 0.9 | 2.9 |
| 159 | 25.1 | 6.3 | 6.3 |

$^a$ $R_{C_6,C_\alpha}$ represents the average distance between the acceptor atom C6 and the $C_\alpha$ atom of the residue. $\Delta\Delta E_{TS}$ denotes the difference in electrostatic interaction energy between the TS and RS, and $\Delta\Delta E_{PS}$ denotes the difference in electrostatic interaction energy between the PS and RS.

decreases the rate of hydride transfer by a factor of 163.[5,7] In our previous hybrid quantum/classical molecular dynamics simulations of the G121V mutant,[27] the free energy barrier increased by an amount that is consistent with this experimentally observed decrease in the hydride transfer rate. The charge deletion scheme identifies Gly-121 and Asp-122 as exhibiting substantial changes in the electrostatic contributions along the collective reaction coordinate. This analysis suggests that the decrease in the hydride transfer rate upon mutation of these residues may arise in part from changes in the electrostatic interactions. Furthermore, a genomic analysis indicates that a number of the residues identified by the charge deletion scheme (e.g., residues 27, 31, 35, 46, 95, 96, 100, 121, and 122 of *E. coli* DHFR) are highly conserved across a wide range of species.[7,26]

**C. Correlated Motions.** Previous analyses of correlated fluctuations for wild-type and mutant DHFR complexes focused on only the reactant and product states,[23,24] although the transition states are expected to strongly impact the behavior of thermally rare events. In this section, we identify correlated fluctuations that characterize the transition state and analyze the impact of these correlated motions on the hydride transfer reaction. The correlated motions associated with a particular

state provide information about the couplings between various regions of the protein but do not provide information about the importance of these couplings for the reaction. Correlations that persist along the reaction coordinate (i.e., from the RS to the TS to the PS) may indicate couplings that are important for maintaining the structural stability but most likely do not provide direct information concerning the reactive event. On the other hand, correlations that change significantly along the reaction coordinate reflect conformational changes that are important for the chemical reaction.

Figure 8 depicts the correlations for the RS, TS, and PS. The PS lacks many of the anticorrelated regions present in the RS. Brooks and co-workers observed a similar reduction in the anticorrelated regions for two Michaelis product structures relative to the reactant state.[23] Although the details of our RS and PS correlation diagrams differ from those of Brooks and co-workers, the qualitative trends are similar. One possible source for the quantitative disparity is the different potential energy surfaces used in the simulations. Furthermore, our definitions of the RS, TS, and PS are based on an ensemble of configurations associated with a particular range of the reaction coordinate, whereas Brooks and co-workers define the RS analogous to an ensemble generated with the pure reactant EVB state (i.e., $\lambda = 0$ in eq 3). We find that a trajectory with $\lambda = 0$ samples a wider range of the reaction coordinate than the range used in our definition of the RS. Despite these differences in the two approaches, they lead to qualitatively similar trends between the RS and PS correlation diagrams. The approach of Brooks and co-workers, however, does not provide a well-defined TS, which is the focus of the present study. As shown in Figure 8, the TS ensemble exhibits correlations that are qualitatively different from those of the RS and the PS ensembles.

We are particularly interested in correlations between motions of distal residues in the TS because experiments indicate that mutation of residues far from the active site can dramatically impact the hydride transfer rate.[7] Figure 9 depicts the cross-correlation as a function of the distance between the $C_\alpha$ atoms for each pair of residues in DHFR for the TS ensemble. While the majority of residue pairs exhibiting significant correlations are located near each other, many residue pairs that are significantly correlated are separated by more than 10 Å. These results provide evidence for the significance of correlated motions between distal residues.

The correlations that are maintained along the reaction coordinate may serve important structural purposes but are not directly relevant to the hydride transfer reaction. Such correlations include residues Met-42 with Ser-63, Met-42 with Gly-97, Ser-63 with Val-75, Gly-67 with Val-88, Val-10 with Ser-63, Ile-2 with Arg-98, His-45 with Ser-148, and Thr-113 with Arg-158. While the majority of these correlations are positive, anticorrelated fluctuations are exhibited for Gly-67 with Val-88, Val-10 with Ser-63, and His-45 with Ser-148. The structural importance of some of the above residues is implicated from the strong hydrogen bonds that are preserved throughout the simulations. Regions that are hydrogen bonded are expected to exhibit correlated motions. For example, Met-42 maintains a hydrogen bond with Ile-60 and Leu-62, and Ser-63 maintains a hydrogen bond with Val-75. This analysis of residues involved in correlated motions that are maintained along the reaction coordinate is also consistent with experimental data. NMR experiments identified unusual dynamic parameters for residues 67−69 and 88 but found that these parameters do not vary among the representative reactant and product DHFR complexes
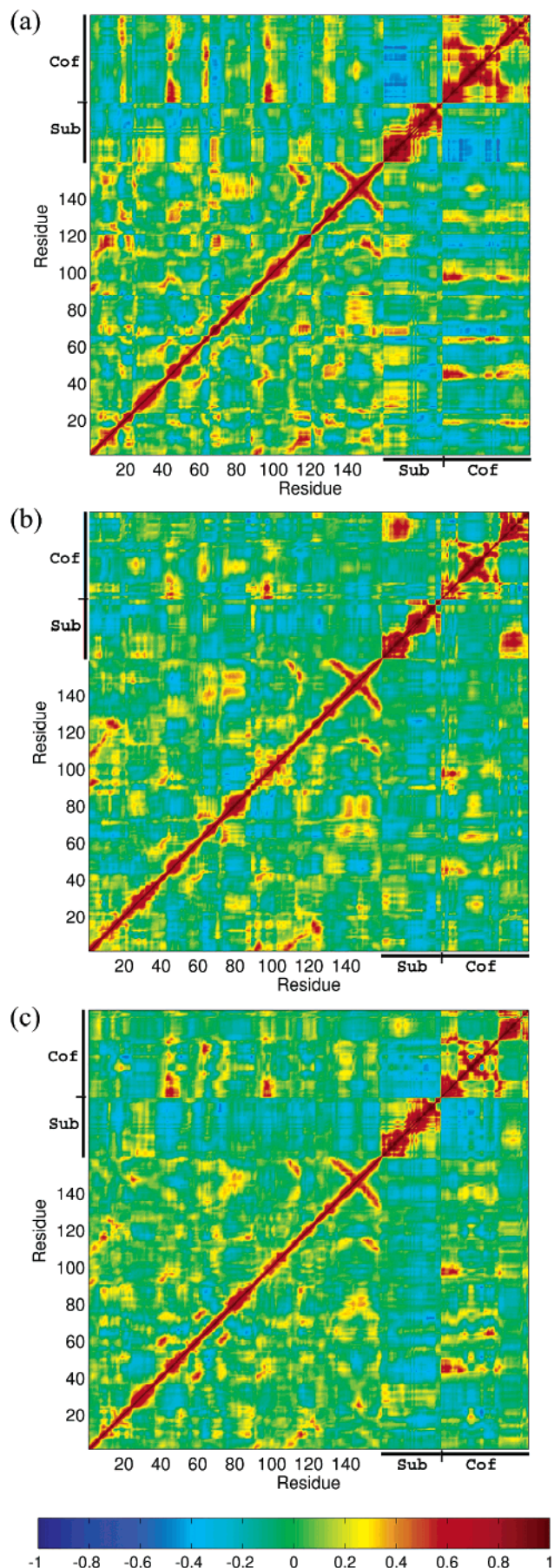
Hydride Transfer in Dihydrofolate Reductase

*J. Phys. Chem. B, Vol. 108, No. 32, 2004*  **12239**



(a)

(b)

(c)

**Figure 8.** Correlation matrix for $C_\alpha$ atoms of the DHFR enzyme and atoms of the substrate and cofactor. Correlated motions are illustrated for (a) RS, (b) TS, and (c) PS ensembles. Positively correlated motions are indicated by red, and anticorrelated motions are indicated by blue.
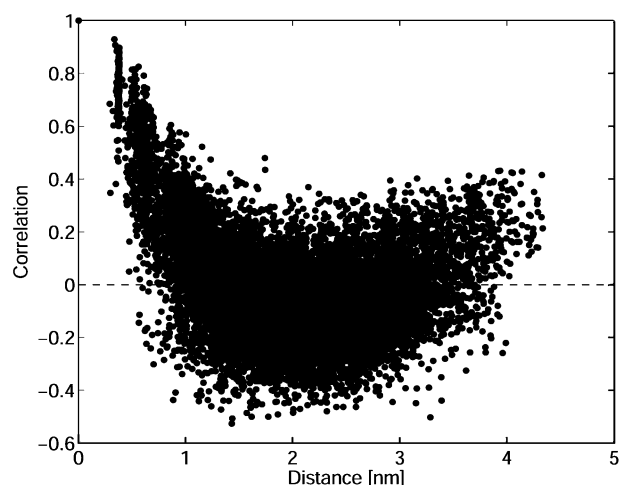


**Figure 9.** The cross-correlation as a function of the distance between the $C_\alpha$ atoms for each pair of residues in DHFR for the TS ensemble.

studied, thereby suggesting that these motions are not directly related to catalysis.[20,46] The observation that mutations of Gly-67 and Val-88 do not significantly alter the hydride transfer rates[47,48] further suggests that the specific motions of these residues do not play a critical role in the hydride transfer reaction.

The correlated motions expected to impact hydride transfer are those that change along the reaction coordinate. While some of the positively correlated regions vanish along the reaction coordinate, the primary change along the reaction coordinate is the disappearance of anticorrelated fluctuations observed in the RS. Many of these vanishing anticorrelated motions occur between distal domains of the protein. For example, the anticorrelated motions between residues of the $\beta$F−$\beta$G loop (residues 117−148) and residues of the Met20 loop (residues 14−24) observed in the RS ensemble are absent in the TS ensemble. The correlations that are positive in the RS but vanish in the TS include the motions between the adenosine binding loop (residues 64−71) and the Met20 loop and motions between the Met20 loop and the $\beta$F−$\beta$G loop. The fluctuations between residues 121−123 and 11−15 become more positively correlated in the TS, suggesting a coupled motion that may be important for the hydride transfer. With respect to the adenosine binding loop, the $\beta$F−$\beta$G loop exhibits both correlated and anticorrelated regions that are present in the RS but either disappear completely or are attenuated in the TS. Of particular interest is the change of phase from anticorrelated fluctuations in the RS to positively correlated fluctuations in the TS between residues 117−120 of the $\beta$F−$\beta$G loop and residues 87−90 of the hinge region. Another trend along the reaction coordinate is observed between Gly-67 and Pro-55, where the correlation changes from a positive value in the RS to a negative value in the PS; these residues are not correlated in the TS. Furthermore, the motion between the hinge region and residues 80−90 is anticorrelated at the TS but is not correlated in the RS and PS. This analysis suggests that the mobility of the hinge region plays a role in the hydride transfer reaction.

In addition to correlations between residues of the protein, Figure 8 also illustrates correlations involving the substrate and cofactor. In the RS, the motion of the pterin ring is anticorrelated with the motion of the NADPH adenosine rings. This anticorrelated motion vanishes in the TS and is significantly attenuated in the PS. In the PS, the motion of the NADPH adenosine rings becomes anticorrelated with the pABG (p-aminobenzoyl-glutamate) ring of the folate. Furthermore, the nicotinamide ring

motion becomes correlated with the pterin ring motion in the TS, as is also observed to a lesser extent in the PS. Even more notable are the changes in the correlations between the protein motions and the motions of the substrate and cofactor. Residues that exhibit a systematic change in the correlation from RS to TS to PS with the motion of the substrate or cofactor include Ala-7, Asn-18, Gly-67, Val-88, Thr-113, Pro-130, and Glu-154. Several of these residues either line the active site or are in close proximity to the substrate and cofactor. In the RS, Gly-67 is positively correlated with the pterin ring of the substrate and anticorrelated with the NADPH adenosine rings, whereas in the TS, Gly-67 is not correlated with the pterin ring of the substrate but is positively correlated with the adenosine rings. The motions of residues Arg-44, Ser-63, and Gly-96 are correlated with the cofactor due to hydrogen bonding interactions.

## IV. Conclusions

In our previous simulations of hydride transfer in DHFR,[25,26] we obtained evidence for a network of coupled promoting motions extending throughout the protein and ligands. These motions represent equilibrium, thermally averaged conformational changes along the collective reaction coordinate and occur on the millisecond time scale of the overall hydride transfer reaction. The network of coupled motions leads to conformations in which the hydride transfer reaction is facilitated because of short transfer distances, suitable orientation of substrate and cofactor, and a favorable electrostatic environment for hydride transfer. In this paper, we characterized this network of coupled motions through analysis of the changes in structure, hydrogen bonding, electrostatic interactions, and correlated motions during the hydride transfer reaction.

The analysis of hydrogen bonding and electrostatics along the collective reaction coordinate provided insight into the impact of conformational changes on the energetics of the reaction. Although the secondary and tertiary structure of the enzyme remained intact along the collective reaction coordinate, significant conformational changes were evident in the loop regions. Concurrent with these conformational changes, a number of hydrogen bonds were observed to break and form along the collective reaction coordinate. In addition, these conformational changes resulted in significant alterations of the electrostatic potential throughout the enzyme. A charge deletion scheme was used to quantify the electrostatic contributions of each residue along the collective reaction coordinate. This electrostatic analysis identified residues throughout the entire enzyme that strongly impact the energetics of the hydride transfer reaction.

Analysis of the correlated motions in the enzyme, cofactor, and substrate revealed significant changes in the correlations along the collective reaction coordinate. Our results are consistent with the previous observation of correlated motions between distal residues.[23] In contrast to previous studies,[23,24] however, we examined the correlation matrix for the transition state ensemble, as well as for the reactant and product state ensembles. As a result, our analysis identified the changes in correlated motions most relevant to hydride transfer. In general, these types of equilibrium correlation analyses are unable to determine if the correlated motions guide the thermally averaged conformational changes of the enzyme during the reaction or are modified as a result of these conformational changes. Nevertheless, the identification of regions with coupled motions that change during the reaction, particularly at the transition state, clarifies the relative importance of previously observed correlated motions for hydride transfer.

In conclusion, these analyses provided insight into how the network of coupled motions facilitates hydride transfer. Key residues with respect to structure, hydrogen bonding, electrostatics, and correlated motions were identified. The changes in electrostatic interaction energies during the reaction play an important role in enzyme catalysis.[53] The significantly varying electrostatic interactions occur throughout the enzyme and are strongly linked to conformational changes along the collective reaction coordinate. These types of analyses are important for protein engineering and drug design.

## References and Notes

(1) Miller, G. P.; Benkovic, S. *J. Chem. Biol.* **1998**, *5*, R105.

(2) Fierke, C. A.; Johnson, K. A.; Benkovic, S. J. *Biochemistry* **1987**, *26*, 4085.

(3) Huang, Z.; Wagner, C. R.; Benkovic, S. J. *Biochemistry* **1994**, *33*, 11576.

(4) Wagner, C. R.; Huang, Z.; Singleton, S. F.; Benkovic, S. J. *Biochemistry* **1995**, *34*, 15671.

(5) Cameron, C. E.; Benkovic, S. J. *Biochemistry* **1997**, *36*, 15792.

(6) Miller, G. P.; Benkovic, S. J. *Biochemistry* **1998**, *37*, 6336.

(7) Rajagopalan, P. T. R.; Lutz, S.; Benkovic, S. J. *Biochemistry* **2002**, *41*, 12618.

(8) Cummins, P. L.; Gready, J. E. *J. Am. Chem. Soc.* **2001**, *123*, 3418.

(9) Shrimpton, P.; Allemann, R. K. *Protein Sci.* **2002**, *11*, 1442.

(10) Shrimpton, P.; Mullaney, A.; Allemann, R. K. *Protein* **2003**, *51*, 216.

(11) Garcia-Viloca, M.; Truhlar, D. G.; Gao, J. *Biochemistry* **2003**, *42*, 13558.

(12) Cummins, P. L.; Gready, J. E. *J. Comput. Chem.* **1990**, *11*, 791.

(13) Andres, J.; Safont, V. S.; Martins, J. B.; Beltran, A.; Moliner, V. *J. Mol. Struct.* **1995**, *330*, 411.

(14) Andres, J.; Moliner, V.; Safont, V. S.; Domingo, L. R.; Picher, M. T.; Krechl, J. *J. Bioorg. Chem.* **1996**, *24*, 10.

(15) Castillo, R.; Andres, J.; Moliner, V. *J. Am. Chem. Soc.* **1999**, *121*, 12140.

(16) Cummins, P. L.; Greatbanks, S. P.; Rendell, A. P.; Gready, J. E. *J. Phys. Chem. B* **2002**, *106*, 9934.

(17) Garcia-Viloca, M.; Truhlar, D. G.; Gao, J. *J. Mol. Biol.* **2003**, *327*, 549.

(18) Sawaya, M. R.; Kraut, J. *Biochemistry* **1997**, *36*, 586.

(19) Falzone, C. J.; Wright, P. E.; Benkovic, S. J. *Biochemistry* **1994**, *33*, 439.

(20) Osborne, M. J.; Schnell, J.; Benkovic, S. J.; Dyson, H. J.; Wright, P. E. *Biochemistry* **2001**, *40*, 9846.

(21) Schnell, J. R.; Dyson, H. J.; Wright, P. E. *Biochemistry* **2004**, *43*, 374.

(22) Verma, C. S.; Caves, L. S. D.; Hubbard, R. E.; Roberts, G. C. K. *J. Mol. Biol.* **1997**, *266*, 776.

(23) Radkiewicz, J. L.; Brooks, C. L., III. *J. Am. Chem. Soc.* **2000**, *122*, 225.

(24) Rod, T. H.; Radkiewicz, J. L.; Brooks, C. L., III. *Proc. Natl. Acad. Sci., U. S. A.* **2003**, *100*, 6980.

(25) Agarwal, P. K.; Billeter, S. R.; Hammes-Schiffer, S. *J. Phys. Chem. B* **2002**, *106*, 3283.

(26) Agarwal, P. K.; Billeter, S. R.; Rajagopalan, P. T. R.; Benkovic, S. J.; Hammes-Schiffer, S. *Proc. Natl. Acad. Sci., U. S. A.* **2002**, *99*, 2794.

(27) Watney, J. B.; Agarwal, P. K.; Hammes-Schiffer, S. *J. Am. Chem. Soc.* **2003**, *125*, 3745.

(28) Warshel, A. *Computer Modeling of Chemical Reactions in Enzymes and Solutions*; John Wiley: New York, 1991.

(29) Billeter, S. R.; Webb, S. P.; Iordanov, T.; Agarwal, P. K.; Hammes-Schiffer, S. *J. Chem. Phys.* **2001**, *114*, 6925.

(30) Billeter, S. R.; Webb, S. P.; Agarwal, P. K.; Iordanov, T.; Hammes-Schiffer, S. *J. Am. Chem. Soc.* **2001**, *123*, 11262.

(31) Benkovic, S. J.; Hammes-Schiffer, S. *Science* **2003**, *301*, 1196.

(32) Thorpe, I. F.; Brooks, C. L., III. *J. Phys. Chem. B* **2003**, *107*, 14042.

(33) van Gunsteren, W. F.; Billeter, S. R.; Eising, A. A.; Hünenberger, P. H.; Krüger, P.; Mark, A. E.; Scott, W. R. P.; Tironi, I. G. *Biomolecular Simulation: The GROMOS96 Manual and User Guide*; Biomos b.v., Zürich and Groningen, VdF Hochschulverlag, ETH Zürich: Zürich, 1996.

Hydride Transfer in Dihydrofolate Reductase

*J. Phys. Chem. B, Vol. 108, No. 32, 2004* **12241**

(34) Webb, S. P.; Hammes-Schiffer, S. *J. Chem. Phys.* **2000**, *113*, 5214.

(35) Iordanov, T.; Billeter, S. R.; Webb, S. P.; Hammes-Schiffer, S. *Chem. Phys. Lett.* **2001**, *338*, 389.

(36) Marcus, R. A. *Annu. Rev. Phys. Chem.* **1964**, *15*, 155.

(37) Zusman, L. D. *Chem. Phys.* **1980**, *49*, 295.

(38) Warshel, A. *J. Phys. Chem.* **1982**, *86*, 2218.

(39) King, G.; Warshel, A. *J. Chem. Phys.* **1990**, *93*, 8682.

(40) Hynes, J. T. In *Theory of Chemical Reaction Dynamics*; Baer, M., Ed.; CRC Press: Boca Raton, FL, Vol. 4; page 171.

(41) Hwang, J.-K.; King, G.; Creighton, S.; Warshel, A. *J. Am. Chem. Soc.* **1988**, *110*, 5297.

(42) Rocchia, W.; Alexov, E.; Honig, B. *J. Phys. Chem. B.* **2001**, *105*, 6507.

(43) Rocchia, W.; Sridharan, S.; Nicholls, A.; Alexov, E.; Chiabrera, A.; Honig, B. *J. Comput. Chem.* **2002**, *23*, 128.

(44) Ichiye, T.; Karplus, M. *Proteins* **1991**, *11*, 205.

(45) Kitao, A.; Go, N. *Curr. Opin. Struct. Biol.* **1999**, *9*, 164.

(46) Epstein, D. M.; Benkovic, S. J.; Wright, P. E. *Biochemistry* **1995**, *34*, 11037.

(47) Miller, G. P. PhD thesis, The Pennsylvania State University, State College, PA 16802, 1997.

(48) Ahrweiler, P.; Frieden, C. *Biochemistry* **1991**, *30*, 7801.

(49) DeLano, W. L. *The PyMol Molecular Graphics System*; DeLano Scientific: San Carlos, CA, 2002.

(50) Humphrey, W.; Dalke, A.; Schulten, K. *J. Mol. Graphics* **1996**, *14*, 33.

(51) Nicholls, A.; Sharp, K. A.; Honig, B. *Proteins* **1991**, *11*, 281.

(52) Nicholls, A.; Bharadwaj, R.; Honig, B. *Biophys. J.* **1993**, *64*, Part2, A166.

(53) Villa, J.; Warshel, A. *J. Phys. Chem. B* **2001**, *105*, 7887.